Signal-processing Challenges in Leveraging 100 Gb/s Wireless THz

Pedro Rodríguez-Vázquez
IHCT, University of Wuppertal
Wuppertal, Germany
rodriguezvazque@uni-wuppertal.de

Marko E. Leinonen
ITEE, University of Oulu
Oulu, Finland
marko.e.leinonen@oulu.fi

Janusz Grzyb
IHCT, University of Wuppertal
Wuppertal, Germany
grzyb@uni-wuppertal.de

Nuutti Tervo
ITEE, University of Oulu
Oulu, Finland
nuutti.tervo@oulu.fi

Aarno Parssinen
ITEE, University of Oulu
Oulu, Finland
aarno.parssinen@oulu.fi

Ullrich R. Pfeiffer
IHCT, University of Wuppertal
Wuppertal, Germany
ullrich.pfeiffer@uni-wuppertal.de

***Abstract*—This paper presents a wireless link based on a Tx and a Rx RF front-end module operating at a LO frequency of 230 GHz. The LO frequency generation paths of the Tx and the Rx are driven using two independent and unlocked frequency synthesizers. Due to this operation mode, the Tx LO leakage is down-converted in the Rx, generating a DC modulated tone that, if not properly handled, will prevent the system to operate appropriately. This paper analyses this effect and presents a solution to mitigate this impairment. Applying this, and using a 16-QAM modulation scheme, a maximum data-rate of 80 Gbps with an EVM of 12.5 % was achieved at a 1-meter distance.**

***Index Terms*—High-speed communications, THz and submm-Wave systems, ultra wideband communication**

I. Introduction

The increasing amount of mobile devices in recent years has increased the demand for wireless data throughput. More bandwidth (BW) is required to satisfy this demand. This can be done by moving the operational carrier frequency higher in the frequency spectrum towards the terahertz bands. Here, the small wavelength allows for a reduction in the form factor of the electrical and electromechanical components, increasing the integration of multiple components within a single chip, including antennas and passives. Expensive III-V semiconductor technologies [1], [2] with low integration capabilities dominated this band in the past. However, the recent advancements in the process technology [3] have made silicon a viable low-cost alternative. Multiple links working above 200 GHz based on SiGe HBT technologies have been published in the recent years, reaching a maximum data-rate of 100 Gbps and a transmission distance of 1-meter [4]–[7], while CMOS-based solutions are lagging behind both in speed and range [8], [9]. Most of these links have been tested under very stable lab set-up, including locked oscillators for Tx and Rx, to ensure frequency and phase alignment in the wireless links.

However, higher distances are expected to be required in the future with the introduction of the IEEE 802.15.3d-2017 standard [10] and the new sixth generation of mobile communications (6G) [11]. These systems operate using independent oscillators for the Tx and the Rx, which presents a significant challenge to direct-conversion systems [4] particularly. This paper presents a wireless link operating at 230 GHz operated with independent and free-running oscillators for the Tx and the Rx. It includes a description of the IQ direct-conversion Tx and the Rx RF front-end modules, their RF characteristics, and an analysis and a solution to the problems generated by a free-running operation mode. After correcting for this, we achieved a peak data-rate of 80 Gb/s with an EVM of 12.5% over a 1-meter distance.

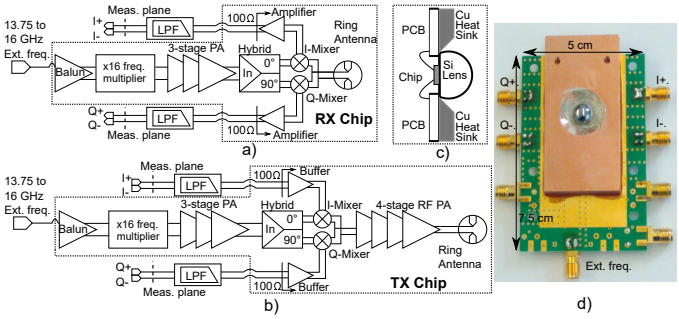

Fig. 1. a) Block diagrams of Rx, b) Tx, c) packaging concept of RF modules and d) photography of the Tx module. [4]

II. Architecture and System Description

A Tx and a Rx RF front-end module were employed to establish the THz wireless communication link. These modules are based on a chipset manufactured in an advanced SiGe HBT technology with f_T/f_{max}=350/550 GHz [3]. Fig. 1 presents the block diagram of the RF front-end modules. Both modules implement a direct-conversion IQ architecture. A 13.75-16 GHz signal from a reference oscillator is fed to an x16 multiplier chain to generate the 220-255 GHz carrier frequency. The x16 multiplier chain is based on 4 cascaded Gilber-cell frequency doublers. A 3-stage power amplifier (PA) amplifies the output signal of the multiplier chain. Afterward, a broadband hybrid [12] is placed to provide a quadrature functionality. A double-

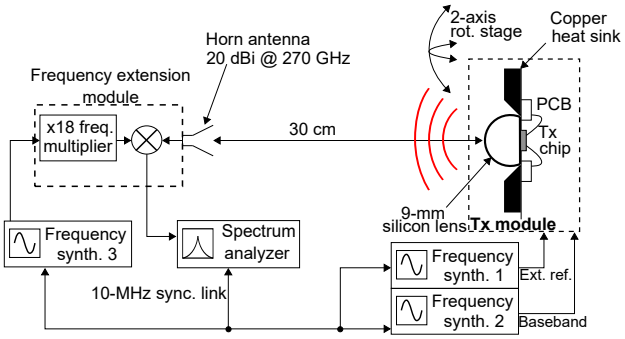

Fig. 2. Free-space measurement set-up for single-tone RF characterization in the transmit mode of operation.

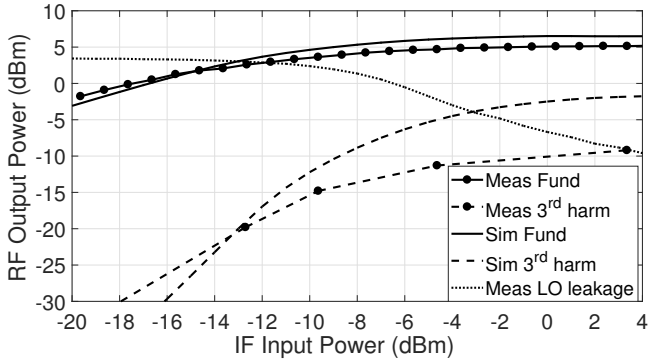

Fig. 3. Tx linearity and total LO leakage for a carrier frequency of 230 GHz and an IF of 5 GHz. The output power is shown per single channel. [4]

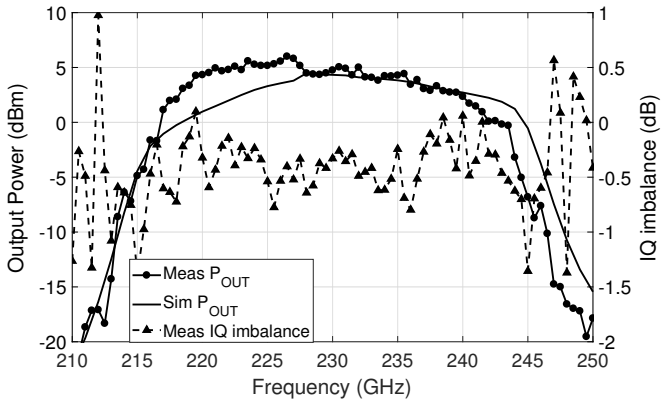

Fig. 4. Tx RF BW, P_{out} and IQ amplitude imbalance for an carrier frequency of 230 GHz and an IF power of -15 dBm. The simulation includes the PCB filters. [4]

balanced IQ Gilbert-cell up-conversion mixer equipped with baseband (BB) buffers for impedance matching is used in the Tx to up-convert the BB signal. The mixer is followed by a 4-stage PA to provide enough output power to the modulated signal. In the Rx, the down-conversion process is realized by a doubled-balanced IQ switching-quad equipped with a set of BB amplifiers to provide enough CG, BB BW, and NF [13]. Both Tx and Rx chips are equipped with a broadband on-chip ring antenna, which radiates through the substrate into a 9-mm high-resistivity silicon-lens. The chip on-lens assembly is glued to the back-side of a high-speed PCB (Rogers 4350B), which includes a cavity to accommodate the chip as well as wire-bond compensation structures for the broadband BB signals.

III. RF Characterization

Both the Tx and Rx modules were characterized independently with a WR-03 (220–325 GHz) frequency extension module from OML, whose output power in the transmit-mode and conversion gain in the receive-mode was first calibrated for further measurements. The OML module was placed in the antenna far-field zone (30 cm). All key Tx and Rx parameters were derived by applying the Friis transmission equation, which involves the antenna directivity on both sides of the measurement set-up. The OML module was equipped with a reference WR-3.4 linearly-polarized conical-horn antenna with a 20-dBi directivity at 270 GHz. The antenna was assumed to be an ideal lossless aperture with the square frequency dependence of its directivity for other frequency points. The appropriate free-space measurement set-up for the transmit mode of operation is shown in Fig. 2. A complimentary set-up was applied for Rx measurements with the spectrum analyzer used to acquire signals at the receiver baseband outputs.

As explained above, the wireless communication link was found to achieve its peak performance at 230 GHz. Therefore the RF measurement results presented here always refer to this carrier frequency. Both Tx and Rx RF modules show a directivity of 26.4 dBi at 230 GHz. The Tx linearity characteristics are presented in Fig. 3 for an IF frequency of 5 GHz. The optimum input power (P_{IN}) for 16-QAM was found to be around the P_{1dB} for BB frequencies up to 10 GHz, resulting in a total IQ radiated P_{OUT} of 4.5 dBm when the system operates in IQ mode. The soft-compression behavior of the Tx (P_{sat}=9 dBm) enables the use of this unusual operating point. Here, the Tx shows a 3-dB RF BW of 28 GHz with an IQ amplitude imbalance below 0.7 dB for the whole BW, as can be observed in Fig 4. The Rx presents a 3-dB RF BW of 26 GHz with a CG of 8 dB. Assuming a thermal noise of 174 dBm/Hz, the minimum single side-band (SSB) NF was estimated to be 14 dB from the measured noise at the Rx output and the previously measured CG. These results are presented in Fig. 5. The Tx dissipates 960 mW, while the Rx only 450 mW. These results have been previously published in [4] and have been included in this paper for completeness.

IV. Wireless Communication Link

A. Measurement set-up description

The Tx and the Rx modules were placed in a 1-meter line-of-sight setup. The setup was completely covered by absorbers to prevent any standing wave or multipath communication. Two differentially-operated arbitrary waveform generators AWG70001A (50 Gs/s each) and two differentially-operated real-time oscilloscopes DPO77002SX (200 Gs/s each) are the main parts of the measurement setup. A PRBS9

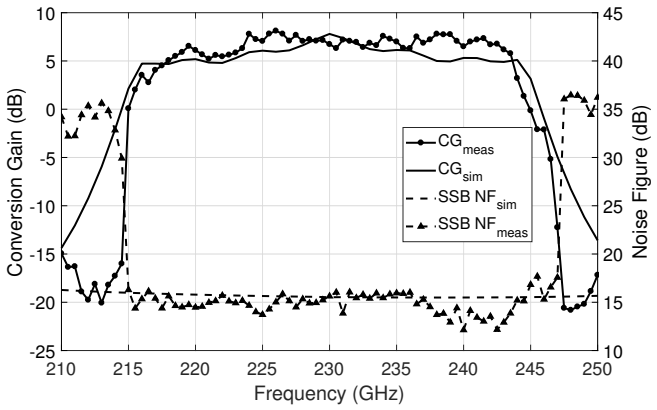

Fig. 5. Rx RF BW, CG, and NF for an carrier frequency of 230 GHz. The simulation includes the PCB filters, limiting the operation BW. [4]

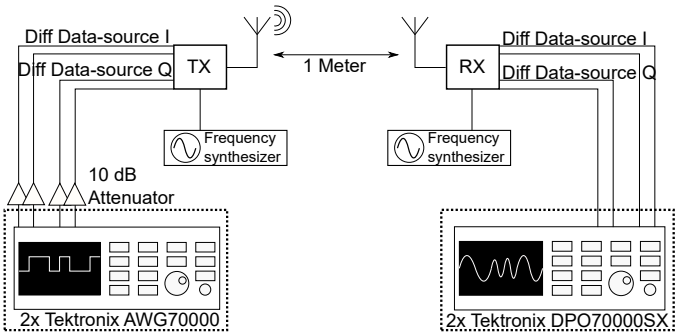

Fig. 6. Diagram of the setup used to characterized the wireless link.

sequence was pulse-amplitude modulated (PAM4) in each of the AWG outputs to generate the complex modulated signal (16-QAM). A root-raised cosine filter with a roll-off factor of 0.35 was applied to the PAM4 signal for pulse shaping and to match the spectral spread of the BB signal with the BW of the Tx and the Rx modules. The AWGs and the scopes were initially connected back to back to analyze this analog BB signal. The BB signal power at different data-rates, its effective bandwidth, defined as the bandwidth that contains 90% of the power of the signal, and the intrinsic EVM error generated by the measurement equipment are depicted in Table I. For data-rates below 50 Gbps the EVM error stays below 1.5 %, and the power delivered by the AWG stays constant at -4.5 dBm. A set of broadband 10 dB attenuators was used to match the measured AWG output power with the linearity curve of the Tx presented in Fig. 3. The received signal was processed

TABLE I
AWG PERFORMANCE.

16-QAM data-rate	Output Power	Effective BW	EVM_{rms}
$\leq$50 Gbps	-4.5 dBm	$\leq$6.9 GHz	$\leq$1.5 %
60 Gbps	-4.7 dBm	8.2 GHz	1.7 %
70 Gbps	-5.2 dBm	9.5 GHz	1.9 %
80 Gbps	-6 dBm	10.7 GHz	2.1 %
90 Gbps	-8.2 dBm	12.4 GHz	2.5 %

in the oscilloscope using a vector signal analysis software (SignalVu). This software analyses EVMs, constellations, and eye diagrams, and facilitates clock recovery and IQ imbalance correction. It also includes an adaptive decision-directed FIR feed-forward equalizer, which was applied to the received signal to compensate for the distortion introduced by the circuits. In this experiment, the number of taps of this filter was set to 101. Unlike in the previous experiments where a maximum data-rate of 100 Gb/s was achieved, the Tx and the Rx LO frequency generation paths were fed using two independent and free-running frequency synthesizers, ensuring their independent operation. A block-diagram of this setup is presented in Fig.6.

B. Digital filter design for LO leakage to DC in RX

The frequency synthesis in the Rx and Tx modules is similar where the incoming reference signal is multiplied four times with a frequency double circuitry inside of the IC, as shown in Fig. 1. The frequency doubling widens the spectrum of the local oscillator (LO) by two in each doubling stage, and the phase noise level of the LO is increased by 3 dB in each frequency doubling stage.

The stability of the oscillator is an important performance parameter of the LO generation. In current wireless telecom systems, the LO of the mobile device (UE) is synchronized to the clock of the base station (BTS) to enhance the accuracy and stability of the LO in UE. If oscillators of UE and BTS are not synchronized, then those can be considered to be running independently. The stability of the oscillator is changed due to the aging of the oscillator [14]. The stability of the oscillator of the used signal generator (SG) can as been modeled with [15]

$$\pm\Delta = \pm\left(r \cdot a + b + c + d\right) \tag{1}$$

where r is the aging rate of the oscillator in years, a is the number of years of operation, b is the temperature change effect, c is the effect of voltage line fluctuation, d is the calibration accuracy. All parameters are in ppm values. The reference signal for the LO generation has been generated with a five years old Keysight E8257 signal generator [15], which operates at 14.375 GHz. The stability Δ of the used SG is $\pm$ 0.19 ppm, and thus the frequency stability of the LO reference signal at 14.375 GHz is $\pm$ 2.73 kHz. The LO chain up-converts the reference LO to 230 GHz with a stability of $\pm$ 43.7 kHz or a frequency instability of 87.4 kHz. The RX module has similar stability, and after the RX down-conversion, the LO leakage instability is $\pm$ 174.8 KHz.

The phase noise of the SG is 16 times wider at the final LO frequency compared to the phase noise at the output of the SG. The measured phase noises of the SG and Tx at the final 230 GHz frequency are presented in Fig. 7.

The limited LO-to-RF port isolation of the Tx modules causes a LO leakage, which is radiated through the antenna. The level of the LO leakage with varying Tx power levels is shown in Fig. 3.

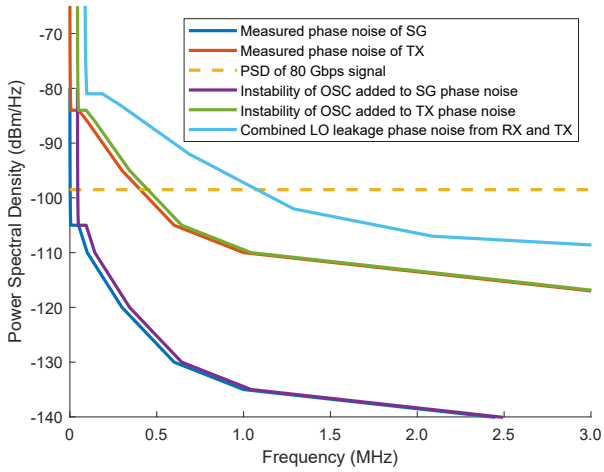

Fig. 7. Phase noises of signal generator, TX and RX in non-synchronized wideband wireless system.

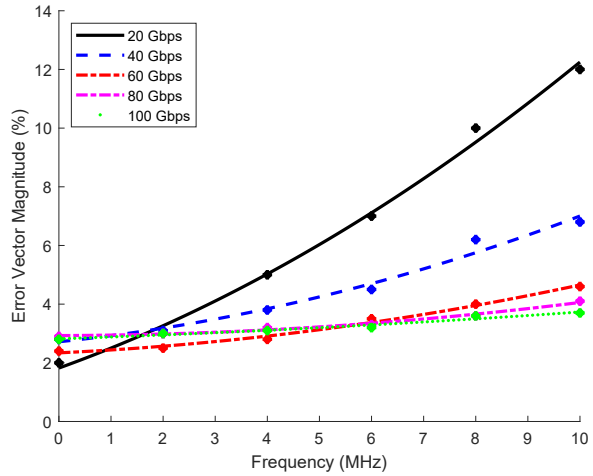

Fig. 8. Effect of digital HP filter BW to signal EVM with various data-rates.

The phase noise level of the combined LO leakage is 3 dB higher than the phase noise level of the Tx since the Rx and the Tx LO leakages are power combined during the down-conversion process. This combined effect of the Tx and the Rx instabilities moves the total phase noise location of the LO leakage at the Rx BB frequency, which is shown in Fig. 7. An 80 Gbps communication with -1.5 dBm Tx level has a two-sided power spectral density of -98.5 dBm, which is shown in Fig. 7. It can be seen that 1.1 MHz wide LO leakage interference is at a higher level than the signal..

The effect of the LO leakage at the Rx BB signal was mitigated with a digital high pass filter, whose -3 dB corner frequency was optimized with respect to EVM with all supported data rates. The optimum of the -3 dB cut-off frequency of the 3rd order high-pass (HP) Butterworth digital filter was found to be 2.0 MHz, as shown in Fig. 8. The digital HP filter was implemented inside of the digital signal processing (DSP) chain of the oscilloscope with a sampling rate of 100 Gs. The DSP of the oscilloscope performs digital signal equalization and EVM calculation for the received signal, as well.

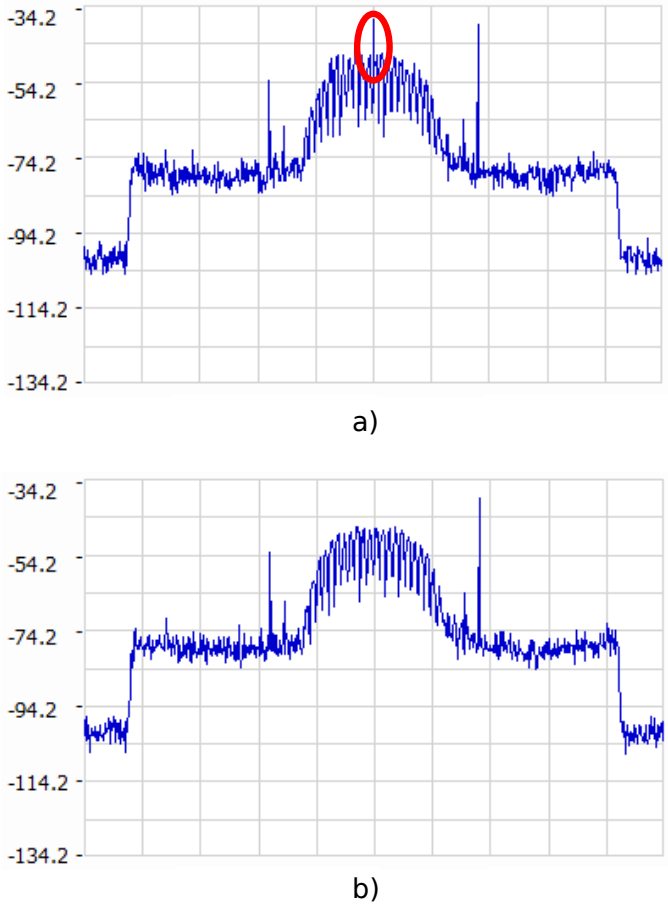

Fig. 9. Spectrum of the a) unfiltered received signal and b) after the the 2 MHz digital LP is applied.

C. Measurement results

The effectiveness of the 2 MHz digital HP filter towards the combined DC leakage due to Tx and Rx LOs is illustrated in Fig.9. Without it, this tone shows a peak power 17 dB above the signal power distribution that would prevent the system from locking. After applying this filter, the wireless communication link was tested for a 16-QAM modulation scheme at 230 GHz. The results are illustrated in Fig. 10. A peak data-rate of 80 Gb/s with an EVM of 12.5% was achieved over a 1-meter distance. A comparison with the current state of the art is presented in Table II.

V. Conclusions

A 1-meter wireless link operating at 230 GHz was presented in this paper. When the multiplier chains at Tx and Rx modules are fed with two independent and free-running signal synthesizers, DSP techniques have to be applied to reduce the influence of the down-converted LO leakage. Under this operating condition, it reaches a peak data-rate of 80 Gbps and an EVM of 12.5%.

TABLE II
WIRELESS LINKS ABOVE 200 GHZ IN SILICON TECHNOLOGY

Ref	Technology	Frequency (GHz)	Modulation	Data-rate (Gbps)	P_{DC} (W)	Efficiency (pJ/b)	LO Locked?	Distance (cm)
[2]	35nm InP HEMT	240	8-QPSK	96	-	-	-	40 m
[1]	80nm InP HEMT	270	16-QAM	100	-	-	-	220
[6]	130nm SiGe	190	BPSK	50	0.154[1]	3[1]	-	0.6
[8]	40nm CMOS	300	16-QAM	32	2.05	65	-	1
[16]	130nm SiGe	225-255	16-QAM	90	1.96/0.98[1]	22/11[1]	Yes	100
[5]	130nm SiGe	220-260	32-QAM	90	1.96/0.98[1]	22/11[1]	Yes	100
[17]	130nm SiGe	220-260	64-QAM	81	1.96/0.98[1]	24/12[1]	Yes	100
[7]	130nm SiGe	240	BPSK	25	0.95	38	-	15
[4]	130nm SiGe	220-255	16-QAM	100	1.41/0.55[1]	14/5.5[1]	Yes	100
This Work	130nm SiGe	230	16-QAM	80	1.41/0.55[1]	1.76/0.69[1]	No	100

[1] Without LO generation circuitry

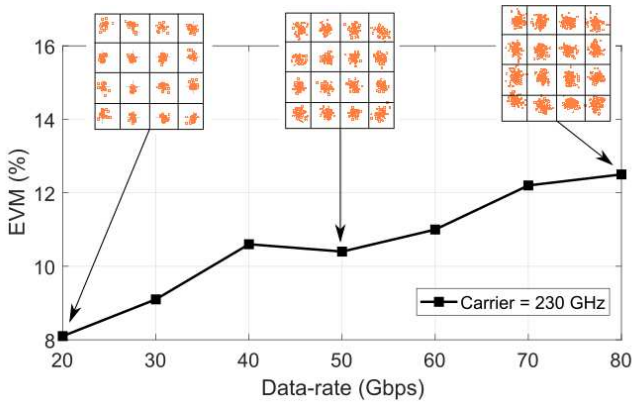

Fig. 10. EVM vs. data-rates measured at 230 GHz.

ACKNOWLEDGEMENT

This work was supported in part by the Academy of Finland 6Genesis Flagship (grant no. 318927), by the German Research Agency (DFG) within the project Real100G.RF (project no. 236714825), and by the European Commission within the project DOTSEVEN (project no. 316755).

REFERENCES

[1] H. Hamada *et al.*, "300-GHz. 100-Gb/s InP-HEMT Wireless Transceiver Using a 300-GHz Fundamental Mixer," in *2018 IEEE/MTT-S International Microwave Symposium - IMS*, June 2018, pp. 1480–1483.

[2] F. Boes *et al.*, "Ultra-broadband MMIC-based wireless link at 240 GHz enabled by 64GS/s DAC," in *2014 39th International Conference on Infrared, Millimeter, and Terahertz waves*, Sept 2014, pp. 1–2.

[3] M. Schroter *et al.*, "The EU DOTSEVEN Project: Overview and Results," in *2016 IEEE Compound Semiconductor Integrated Circuit Symposium (CSICS)*, Oct 2016, pp. 1–4.

[4] P. Rodríguez-Vázquez, J. Grzyb, B. Heinemann, and U. R. Pfeiffer, "A 16-QAM 100-Gb/s 1-M Wireless Link With an EVM of 17GHz in an SiGe Technology," *IEEE Microwave and Wireless Components Letters*, vol. 29, no. 4, pp. 297–299, April 2019.

[5] P. Rodríguez-Vázquez, J. Grzyb, B. Heinemann, and U. R. Pfeiffer, "Performance Evaluation of a 32-QAM 1-Meter Wireless Link Operating at 220 260 GHz with a Data-Rate of 90 Gbps," in *2018 Asia-Pacific Microwave Conference*, Nov 2018, pp. 723–725.

[6] D. Fritsche, P. Stärke, C. Carta, and F. Ellinger, "A Low-Power SiGe BiCMOS 190-GHz Transceiver Chipset With Demonstrated Data Rates up to 50 Gbit/s Using On-Chip Antennas," *IEEE Transactions on Microwave Theory and Techniques*, vol. 65, no. 9, pp. 3312–3323, Sept 2017.

[7] M. H. Eissa *et al.*, "Wideband 240-GHz Transmitter and Receiver in BiCMOS Technology With 25-Gbit/s Data Rate," *IEEE Journal of Solid-State Circuits*, pp. 1–11, 2018.

[8] S. Hara *et al.*, "A 32Gbit/s 16QAM CMOS receiver in 300GHz band," in *2017 IEEE MTT-S International Microwave Symposium (IMS)*, June 2017, pp. 1703–1706.

[9] S. V. Thyagarajan, S. Kang, and A. M. Niknejad, "A 240 GHz Fully Integrated Wideband QPSK Receiver in 65 nm CMOS," *IEEE Journal of Solid-State Circuits*, vol. 50, no. 10, pp. 2268–2280, Oct 2015.

[10] "IEEE standard for high data rate wireless multi-media networks–amendment 2: 100 Gb/s wireless switched point-to-point physical layer," *IEEE Std 802.15.3d-2017 (Amendment to IEEE Std 802.15.3-2016 as amended by IEEE Std 802.15.3e-2017)*, pp. 1–55, Oct 2017.

[11] M. Latva-aho and K. Lepannen, "Key drivers and research challenges for 6G ubiquitous wireless intelligence," pp. 1–13, 2019.

[12] J. Grzyb, K. Statnikov, N. Sarmah, and U. R. Pfeiffer, "A Wideband 240 GHz Lens-Integrated Circularly Polarized On-Chip Annular Alot Antenna for a FMCW Radar Transceiver Module in SiGe Technology," in *2015 SBMO/IEEE MTT-S International Microwave and Optoelectronics Conference (IMOC)*, Nov 2015, pp. 1–4.

[13] P. Rodríguez Vázquez, J. Grzyb, N. Sarmah, B. Heinemann, and U. Pfeiffer, "A 219-266 GHz LO-tunable direct-conversion IQ receiver module in a SiGe HBT technology," *IJMWT*, vol. 10, pp. 587–595, 2018.

[14] R. L. Filler and J. R. Vig, "Long-term aging of oscillators," *IEEE Transactions on Ultrasonics, Ferroelectrics, and Frequency Control*, vol. 40, no. 4, pp. 387–394, July 1993.

[15] *Data sheet Agilent E8257D PSG Microwave Analog Signal Generator*, Keysight, 08 2012.

[16] P. Rodríguez-Vázquez, J. Grzyb, N. Sarmah, B. Heinemann, and U. R. Pfeiffer, "Towards 100 Gbps: A Fully Electronic 90 Gbps One Meter Wireless Link at 230 GHz," in *2018 48th European Microwave Conference (EuMC)*, Sep. 2018, pp. 1389–1392.

[17] P. Rodrguez-Vzquez, J. Grzyb, B. Heineman, and U. R. Pfeiffer, "Optimization and Performance Limits of a 64-QAM Wireless Communication Link at 220-260 GHz in a SiGe HBT Technology," in *2019 IEEE Radio and Wireless Symposium (RWS)*, Jan 2019, pp. 1–3.